Electronic Supplementary Material (ESI) for RSC Advances.

Supplementary Information for High-Performance Breath Acetone Sensor of an Indispensable $V_4C_3T_x$ MXene

Wei-Na Zhao,*[a] Na Yun,[b] Zhen-Hua Dai,[a] and Ye-Fei Li *[c]

[a] Guangzhou Key Laboratory of Environmental Catalysis and Pollution Control, Guangdong Key Laboratory of Environmental Catalysis and Health Risk Control, Institute of Environmental Health and Pollution Control, School of Environmental Science and Engineering, Guangdong University of Technology, Guangzhou 51006, China

[b]School of Chemical Engineering and Technology, Guangdong Industry Polytechnic, Guangzhou 510300, China

[c] School Collaborative Innovation Center of Chemistry for Energy Material, Key Laboratory of Computational Physical Science (Ministry of Education), Shanghai Key Laboratory of Molecular Catalysis and Innovative Materials, Department of Chemistry, Fudan University, Shanghai 200433, China

METHODS

XRD analyses of V_4AlC_3 and $V_4C_3T_x$. The powder XRD patterns were collected using a Rigaku DMAX 2500 diffractometer with monochromatized Cu-Kα radiation at room temperature in the 2θ range of 5–50° with a scan step width of 0.05°. The measured X-ray powder diffraction patterns of V_4AlC_3 were compared with that of $V_4C_3T_x$ as shown in Figure 2c.

SEM and EDX analyses of V_4AlC_3 and $V_4C_3T_x$. SEM and semiquantitative microprobe analyses (Table S1, S2) on $V_4C_3T_x$ and its parent, V_4AlC_3 were performed with the aid of a field emission scanning electron microscope (JSM-5410) equipped with an energy dispersive X-ray spectroscope (EDX, Oxford INCA).

TEM and EDX analyses of $V_4C_3T_x$ nanosheets. A transmission electron microscope (JEOL JEM-2100F) coupled with energy dispersive X-ray spectroscopy (EDS) was used to take the transmission electron microscopy (TEM) images, EDX spectra and elemental mappings of $V_4C_3T_x$ nanosheets. The Z-contrast STEM imaging were done with a modified JEOL 2100F with delta probe corrector, which corrects the aberration up to 5th order, resulting in a probe size of 1.4 A. The imaging was conducted at an acceleration voltage of 60 kV. The convergent angle for illumination is about 35 mrad, with a collection detector angle ranging from 62 to 200 mrad.

XPS characterizations of $V_4C_3T_x$ MXene. The $V_4C_3T_x$ powder were investigated by X-ray photoelectron spectroscopy (XPS). The XPS spectra were acquired using a monochromated Al Kα source ($h\nu$ = 1486.7 eV) connected to a UHV cluster system described elsewhere. An analyzer acceptance angle of (±8°, a take-off angle of ±45°, and pass energy of 15 eV were used for this study. The measured XPS spectra were shown in Figure S4 and S5.

Determination of surface area of $V_4C_3T_x$ nanosheet. The Brunner-Emmett-Teller (BET) method was applied to determine surface area of $V_4C_3T_x$ nanosheets and the corresponding measurement was performed on a Micromeritics ASAP 2020 instrument at 77K. The testing results of N_2 adsorption–desorption isotherms of $V_4C_3T_x$ nanosheets and the corresponding fitting line were shown in Figure S7a and S7b. The details of BET calculation are given as follows:

BET equation:
$$v = \frac{cxv_m}{(1-x)[1+(c-1)x]} \quad \text{(Eq. S1)}$$

Where $x = P/P_0$, v is the volume of nitrogen adsorbed per gram of $V_4C_3T_x$ nanosheets, v_m is the monolayer capacity, and c is related to the heat of adsorption.

The equation can be rewritten in the form:

$$\frac{P}{v(P_0-P)} = \frac{x}{v(1-x)} = \frac{1}{v_m c} + \frac{(c-1)x}{v_m c} \quad \text{(Eq. S2)}$$

Based on the fitting line (Figure S6b), the slope and y-intercept of the line yield c = 51.4 and v_m = 32.5 cm^3/g.

The surface area is calculated from:

$$A = v_m N_{av} \sigma_0 \qquad \text{(Eq. S3)}$$

Where σ_0 is the cross-sectional area of nitrogen at liquid density and N_{av} is Avogadro's number.

So the resulting surface area of $V_4C_3T_x$ nanosheets is 156 m^2/g.

Electrical transport of $V_4C_3T_x$ film. Electrical transport of $V_4C_3T_x$ film was measured with the four-point probe method in a quantum Design PPMS with a Delta-mode method by a Keithley 6221 current source meter and a 2182A nanovoltmeter from 3K to 300 K.

Gas sensing test of $V_4C_3T_x$ sensor in high humidity. The response of acetone, ethanol, toluene, ammonia, nitrogen dioxide, carbon dioxide and benzene were tested under humidity of RH ~ 90%. The experimental setup is illustrated as Figure S21. A total flow of 1000 sccm dry air was divided into two streams, passing through two bubblers, respectively. The first bubbler was filled with deionized water, while the second bubbler was filled with deionized water mixed with acetone (or ethanol, or toluene, or ammonia, or nitrogen dioxide, or carbon dioxide, or benzene). Assuming a full saturation of all vapors, the acetone or other gased concentration in the second bubbler can be estimated by considering their mixture ratios, vapor pressures. Assume ideal gas law, the acetone vapor concentration in the second bubbler could be estimated by

$$X\ (ppm) = \frac{P_V(acetone) \times 10^6}{(Pv(acetone) + Pv(water) + Pv(air)) \times (V(water)/V(acetone))}$$

Where P_v (acetone) stands for the vapor pressure of acetone, P_v (water) stands for the vapor pressure of water and P_v(air) stands for the vapor pressure of air.

V(water)/*V*(acetone) stands for the volume ratio between water and acetone in their mixture.

For calculation, we assume standard air pressure of 760 mmHg. The vapor pressure of acetone at 25 °C was assigned to 231 mmHg[1], the vapor pressure of water at 25 °C was assigned to 23.8 mmHg[2]. From the equation, one can find that a mixture ratio of V(water) : V(acetone) = 1 : 1138 is required to obtain 200 ppm of acetone vapor in the second bubbler.

The vapor pressure of ethanol, and toluene at 25 °C could be assigned to 59.3 mmHg[3] and 28.4 mmHg[3], respectively. Similarly, we can calculate that *V*(water) : *V*(ethanol) = 1 : 352 is needed to get 200 ppm of ethanol vapor in the second bubbler, and *V*(water) : *V*(toluene) = 1: 175 is needed to get 200 ppm of toluene vapor in the second bubbler.

The Volatile Organic Compound (VOC) concentration could be adjusted between 0 and 200 ppm by varying the flow ratio between the first and the second bubbler. First of all, the resistance of $V_4C_3T_x$ sensor under air back ground was investigated as compared to the nitrogen background gas. As shown in Figure S22, it is noted that when the background was switched from N_2 to dry air, the resistance under dry air will increase by 20 %, which is probably caused by the doping of oxygen. The sensing responses of $V_4C_3T_x$ sensor in 25 ppm, 50 ppm, 100 ppm and 200 ppm acetone were also measured and in order to compare their relative percentile resistance changes conveniently, all the curves were plotted to the same scale, as shown in Figure S23. In addition, we also checked the response of $V_4C_3T_x$ sensor in different chemicals including acetone, ethanol, toluene, ammonia, nitrogen dioxide, carbon dioxide and benzene (Figure S24 and S25), displaying that acetone has the highest response in different gases.

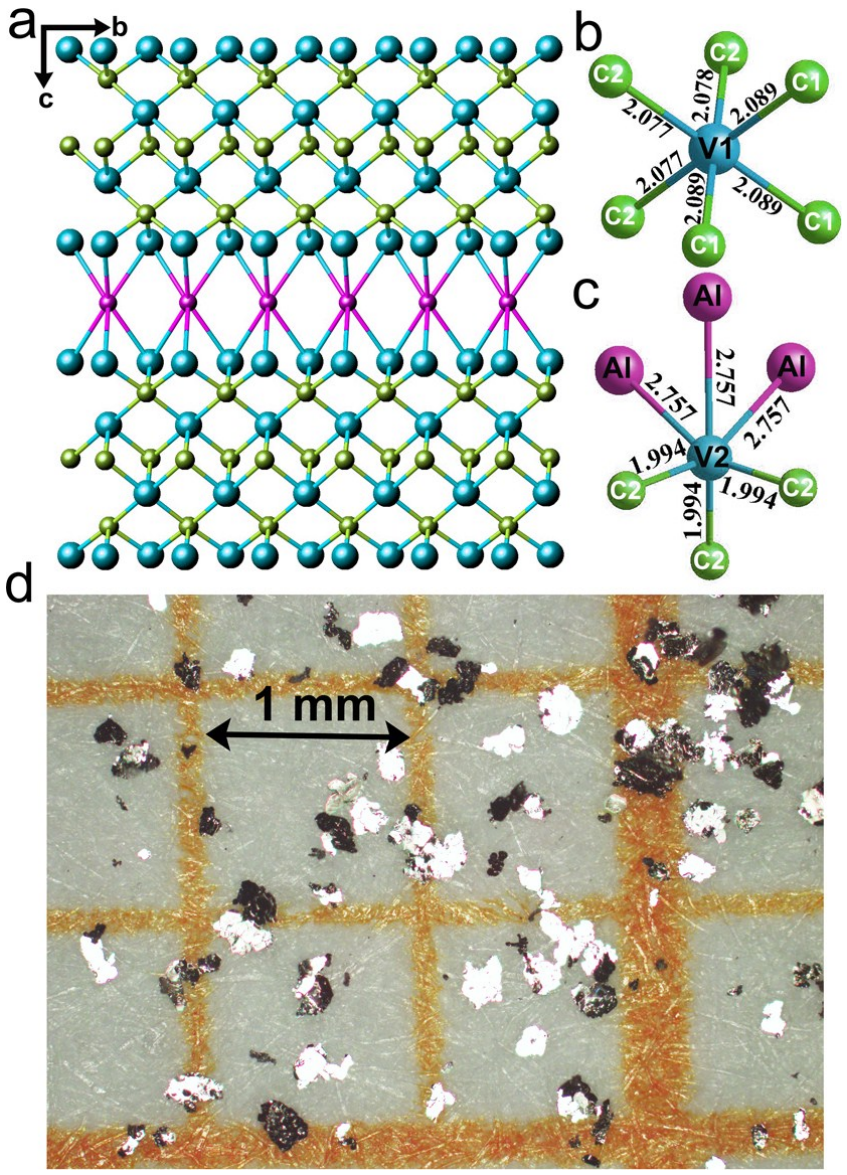

Figure S1. **The crystal structure of V_4AlC_3**. (a) Crystal structure of V_4AlC_3 along *a* axis. Local coordination circumstance around V1 (b) and V2 (c) atoms for V_4AlC_3, and the bond distances (Å) are marked. (d) The optical image of V_4AlC_3 single crystals.

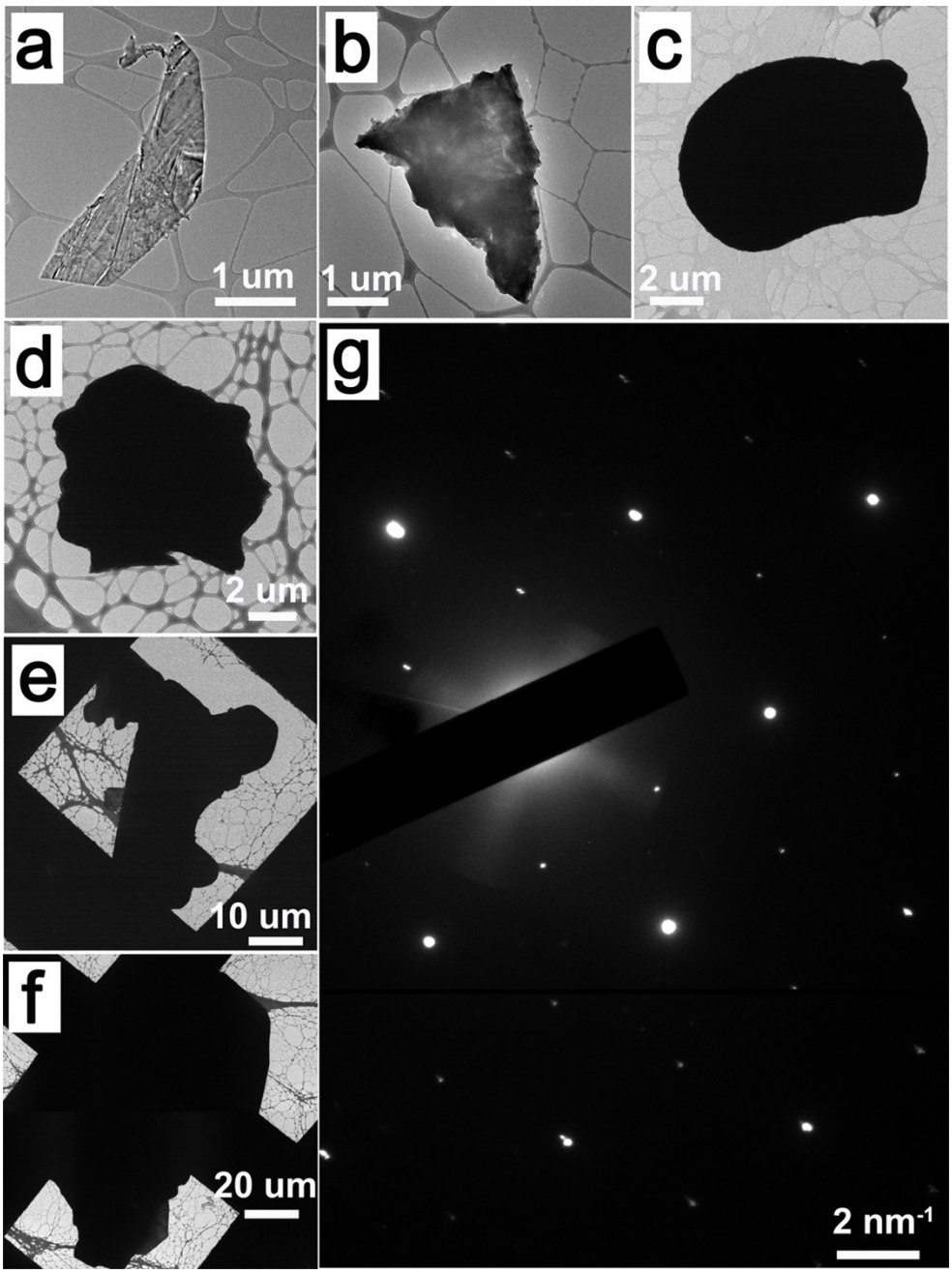

Figure S2. **TEM characterization of V_4AlC_3 single crystals**. (a–f) Low-magnification TEM images of V_4AlC_3 single crystals with different thicknesses and the lateral sizes in the range of several to several hundred microns. (g) The transmission electron diffraction pattern of V_4AlC_3 single crystals along the [001] zone axis, showing good single-crystal diffraction spots.

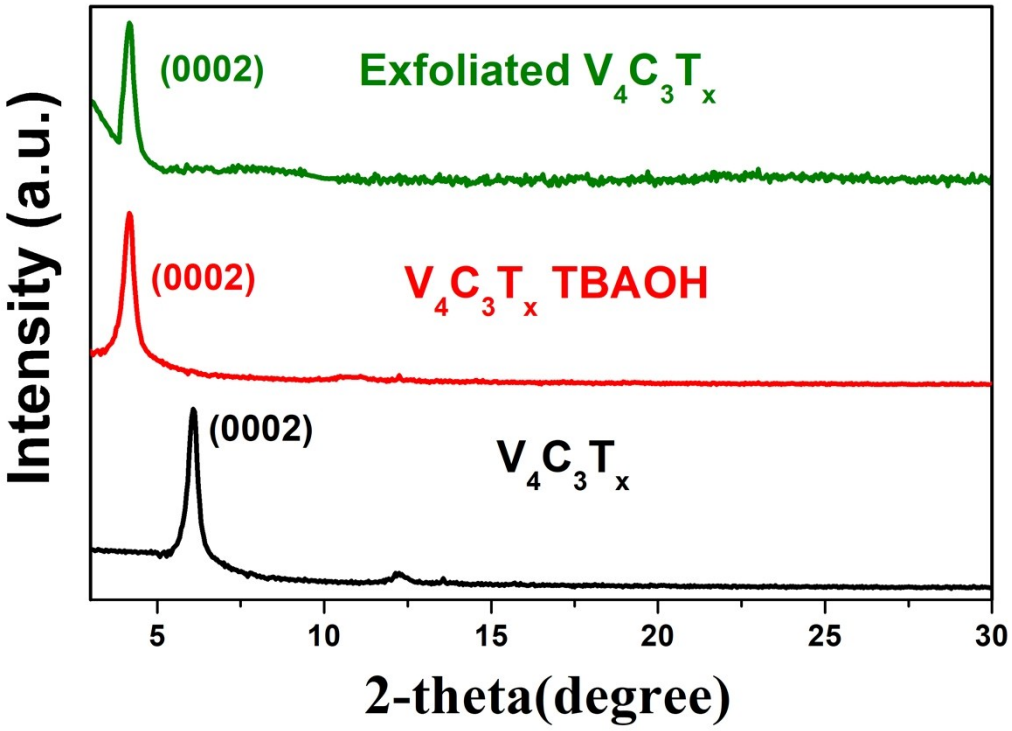

Figure S3. XRD patterns of V_4C_3Tx before and after TBAOH treatment (bottom and middle), and the corresponding exfoliated nanosheets produced by sonication (top)

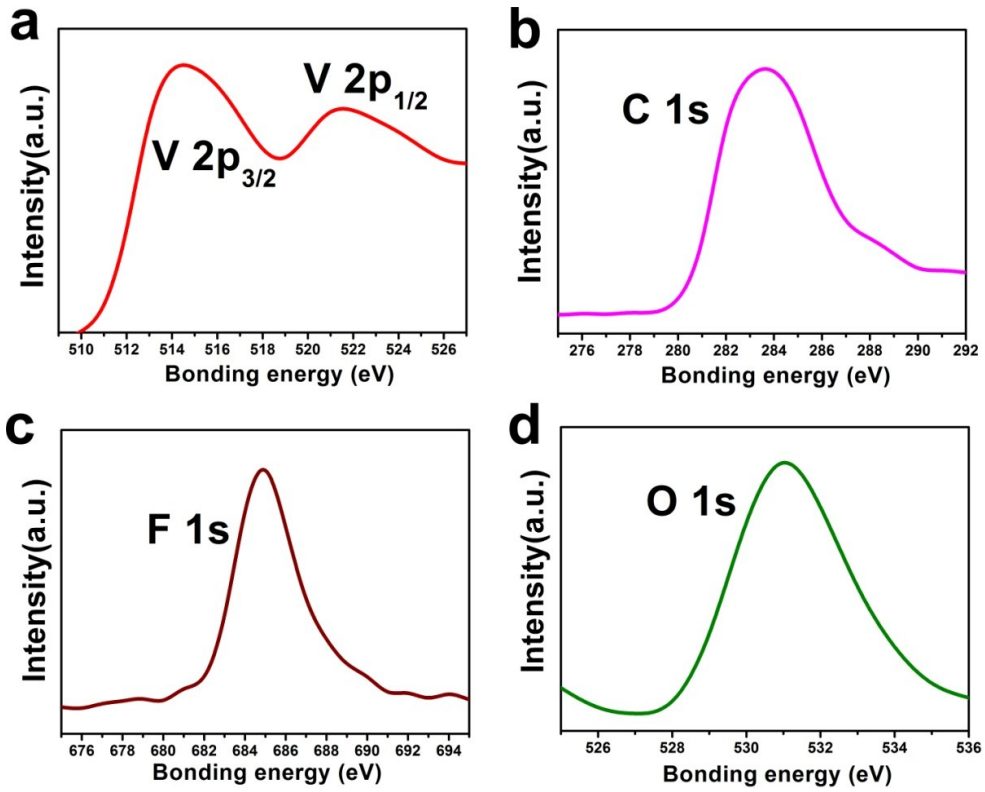

Figure S4. **XPS spectra of V 2p, C 1s, F 1s and O 1s in $V_4C_3T_x$**. XPS spectra of V 2p (a), C 1s (b),F 1s (c) and O 1s (d). V : C : F : O ratio calculated from high-resolution elemental XPS spectra from V 2p, C 1s, F 1s and O1s regions confirms a V : C : F : O ratio of 4 : 3.24 : 1.58 : 5.54, displaying the V–C framework is completely preserved after HF treatment.

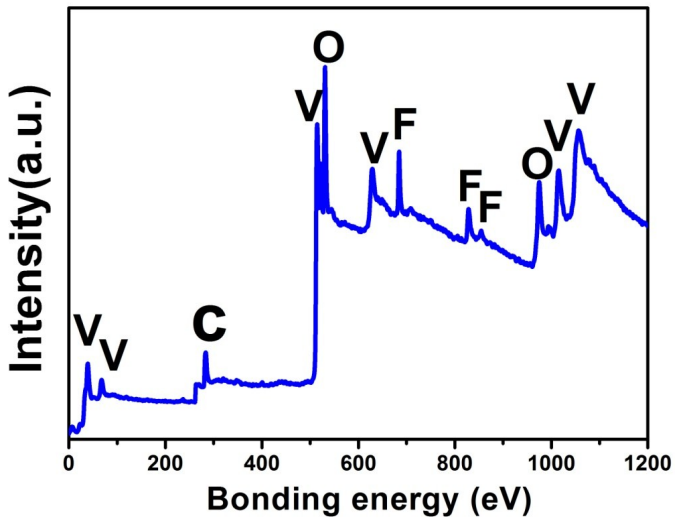

Figure S5. **XPS characterization of $V_4C_3T_x$**. XPS spectrum of $V_4C_3T_x$. Four elements are present: V, C, F and O.

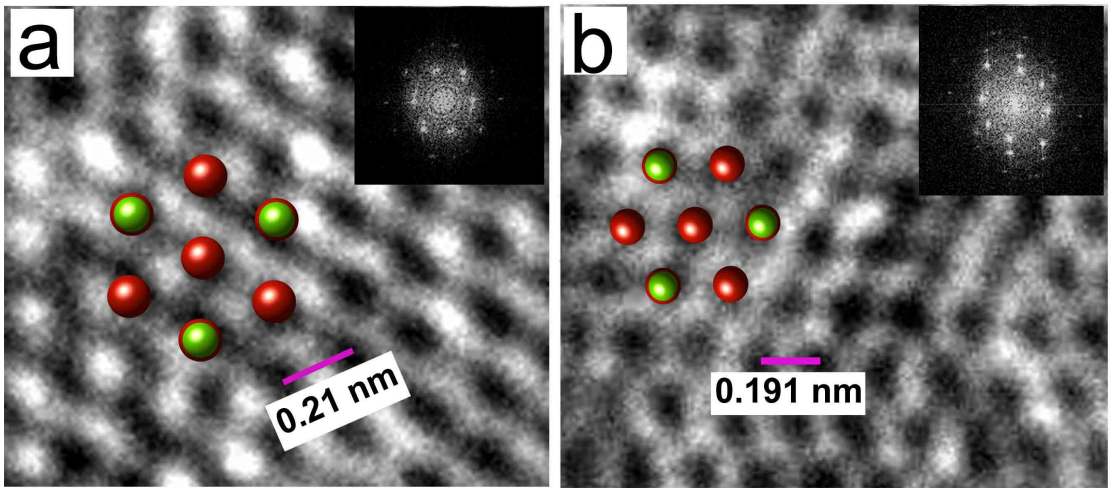

Figure S6. High-resolution TEM images of $V_4C_3T_x$ nanosheets (a) and quantum dots (b) and corresponding FFT patterns are shown in the insets.

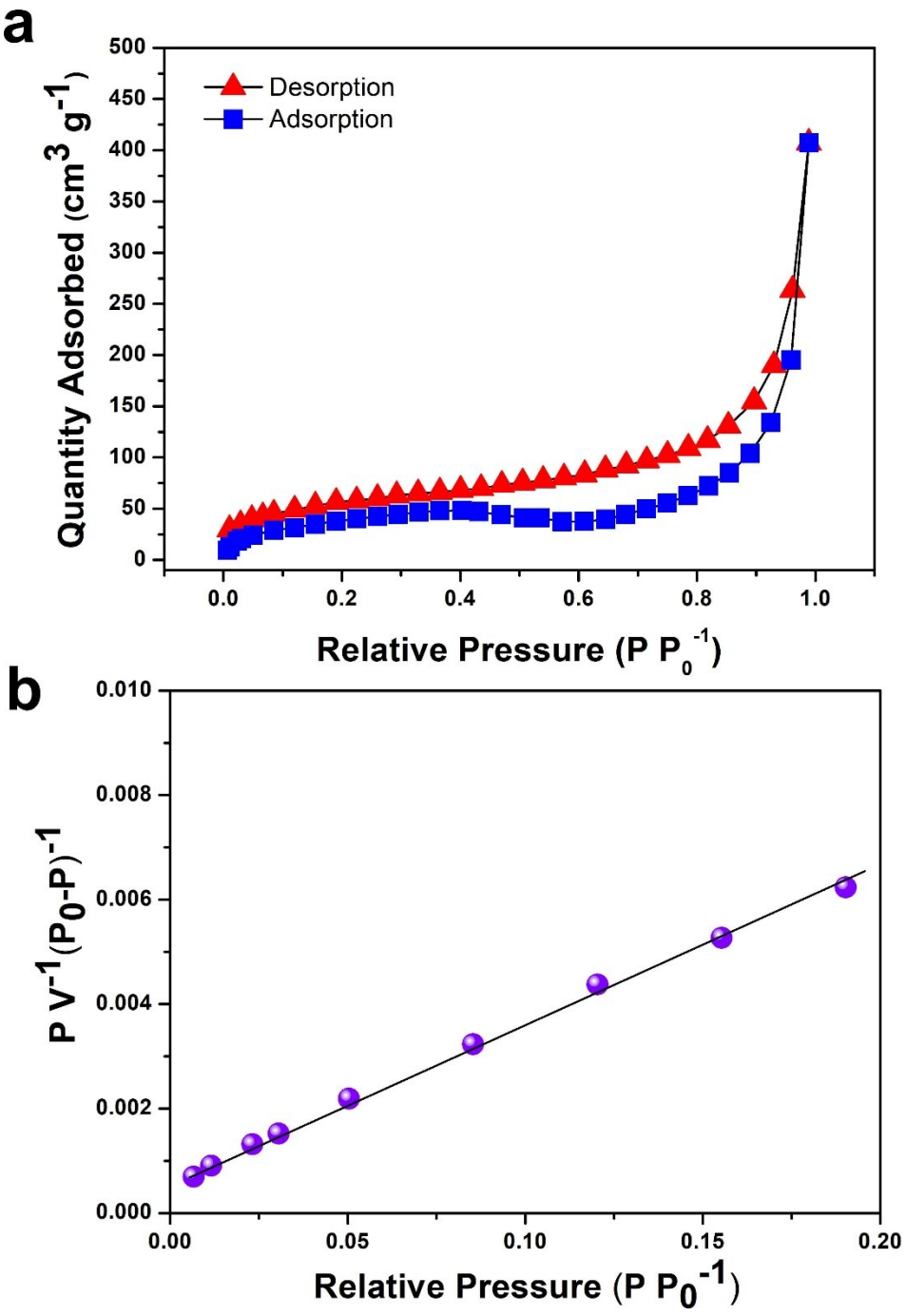

Figure S7. (a) N_2 adsorption–desorption isotherms of $V_4C_3T_x$ nanosheets at 77 K. (b) The fitting line of the low-pressure isotherm data.

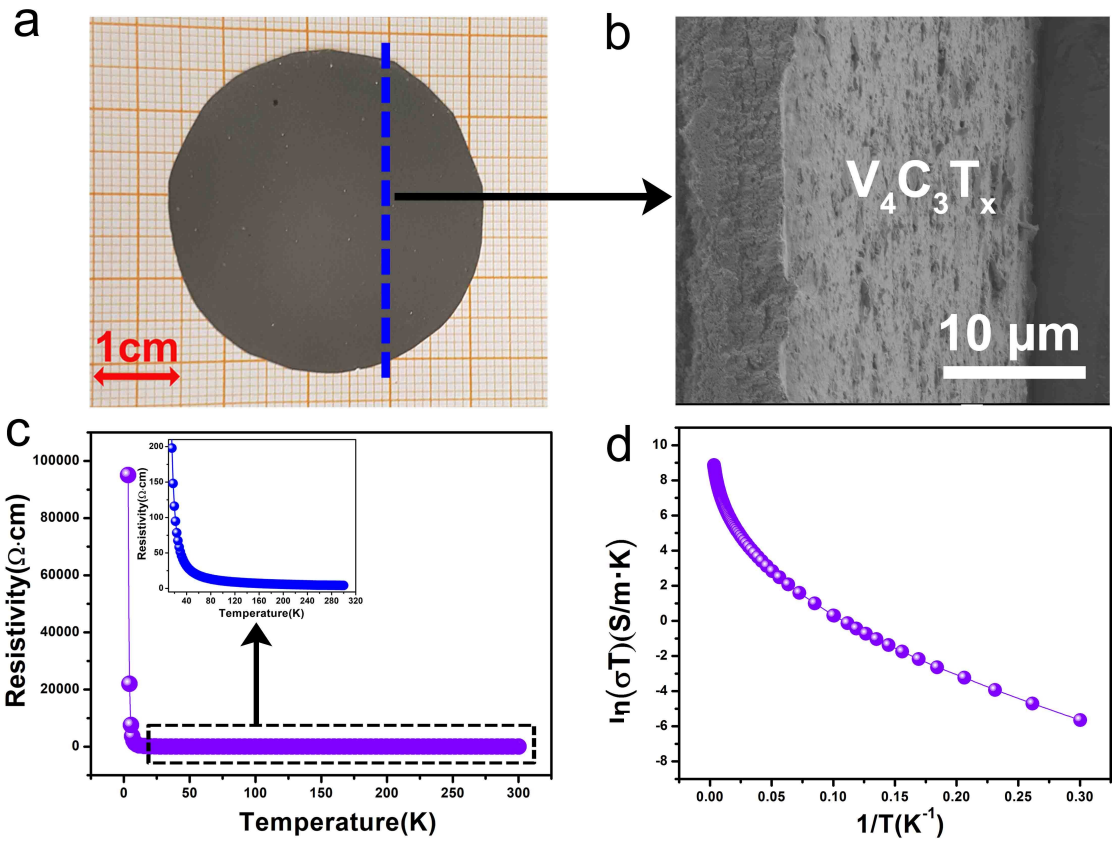

Figure S8. **The electrical performance of as-fabricated $V_4C_3T_x$ film.** (a) A thick film of as-exfoliated $V_4C_3T_x$ nanosheets prepared by vacuum filtration. (b) The cross-sectional SEM image of $V_4C_3T_x$ film with thickness about 18 μm. (c) The resistivity with dependence of temperature (3–300K) of as-fabricated $V_4C_3T_x$ film, the insets are the curve of the resistivity VS temperature from 20K to 300K. (d) Arrhenius plot of the conductivity of as-exfoliated $V_4C_3T_x$ nanosheets.

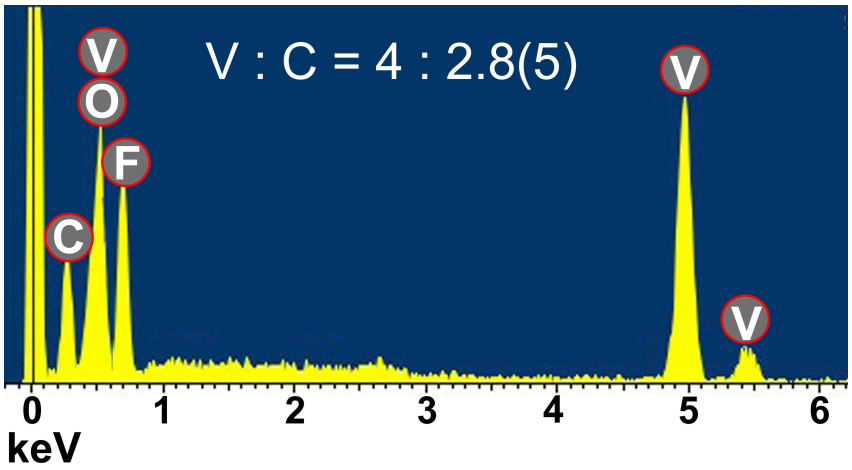

Figure S9. EDS result of $V_4C_3T_x$ nanodots, implying that the basic V-C framework was completely remained when MAX was transformed into MXene nanodots.

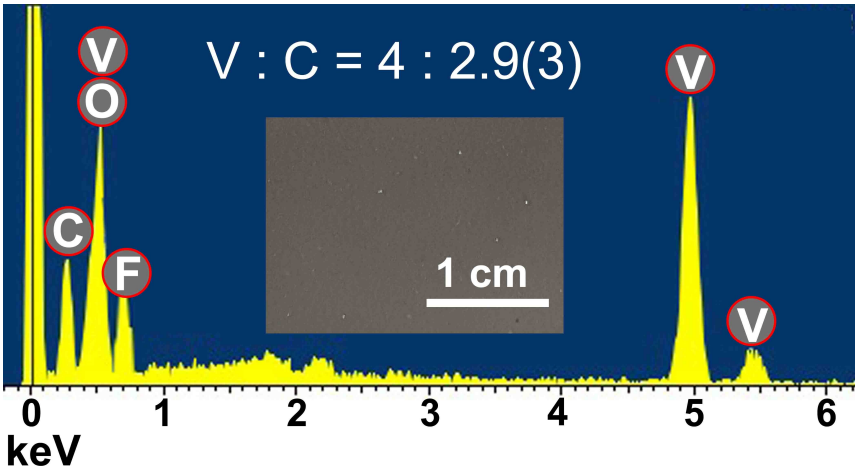

Figure S10. EDS result of $V_4C_3T_x$ film (inset) produced by filtration of as-etched samples, implying that MAX has been completely transformed into MXene.

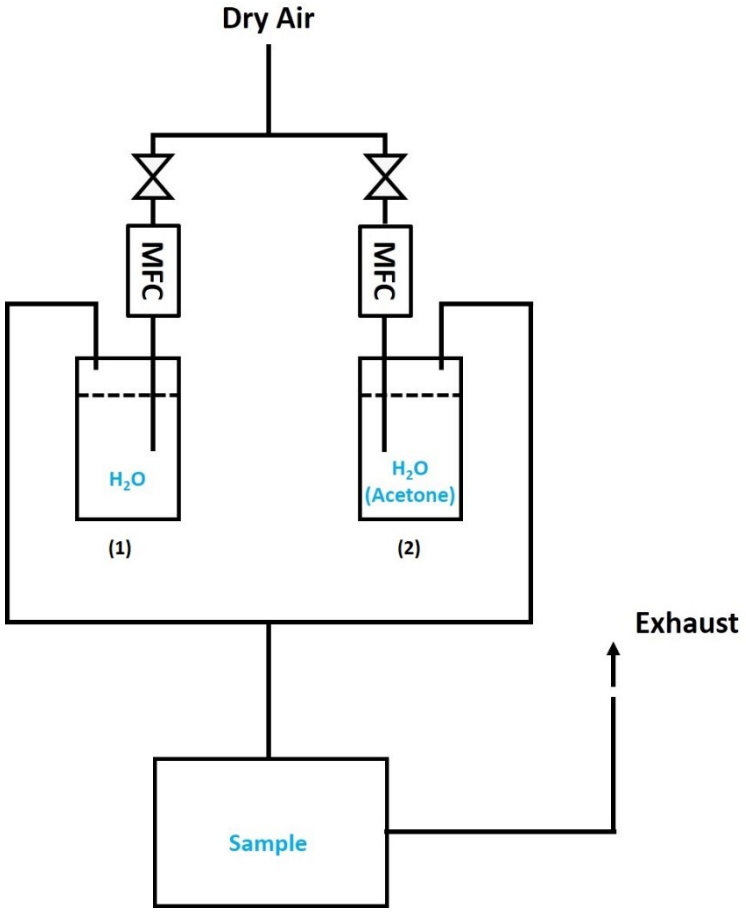

Figure S11. Experimental setup of VOC test at high humidity

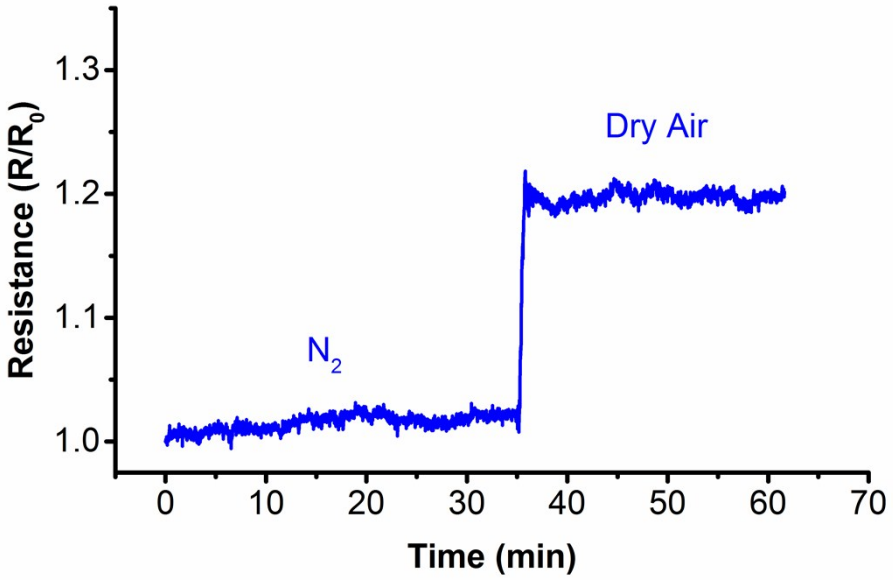

Figure S12. Resistance of $V_4C_3T_x$ sensor under N_2 and dry air background gas.

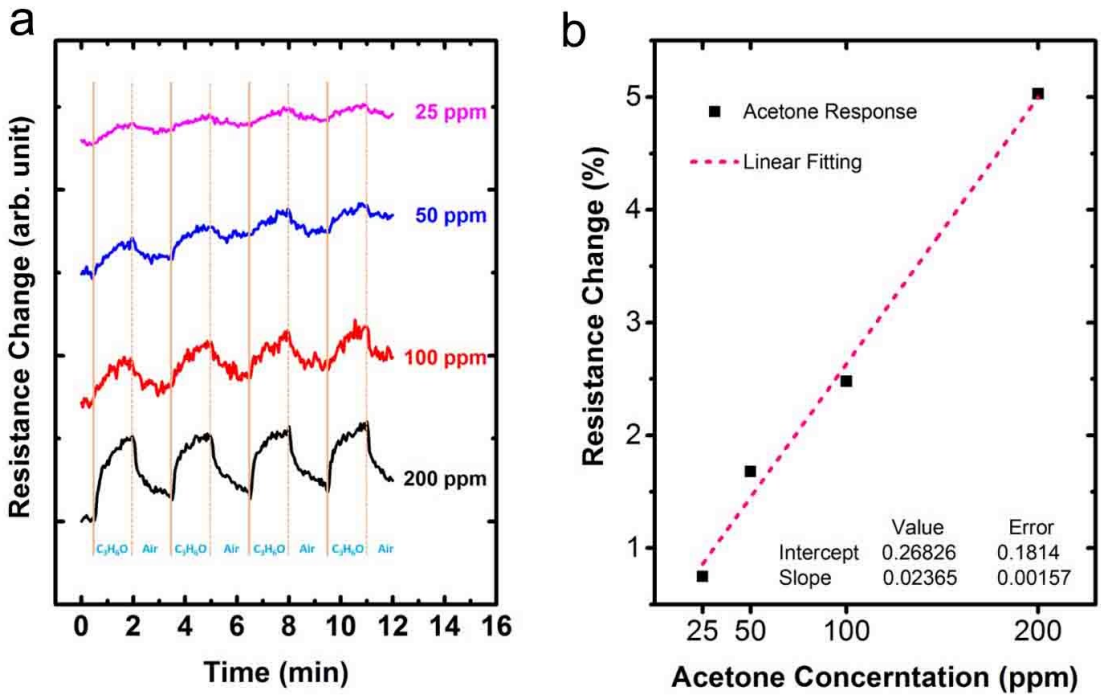

Figure S13. (a) Resistance of $V_4C_3T_x$ film at different acetone concentration. (b) The linear fitting of acetone response.

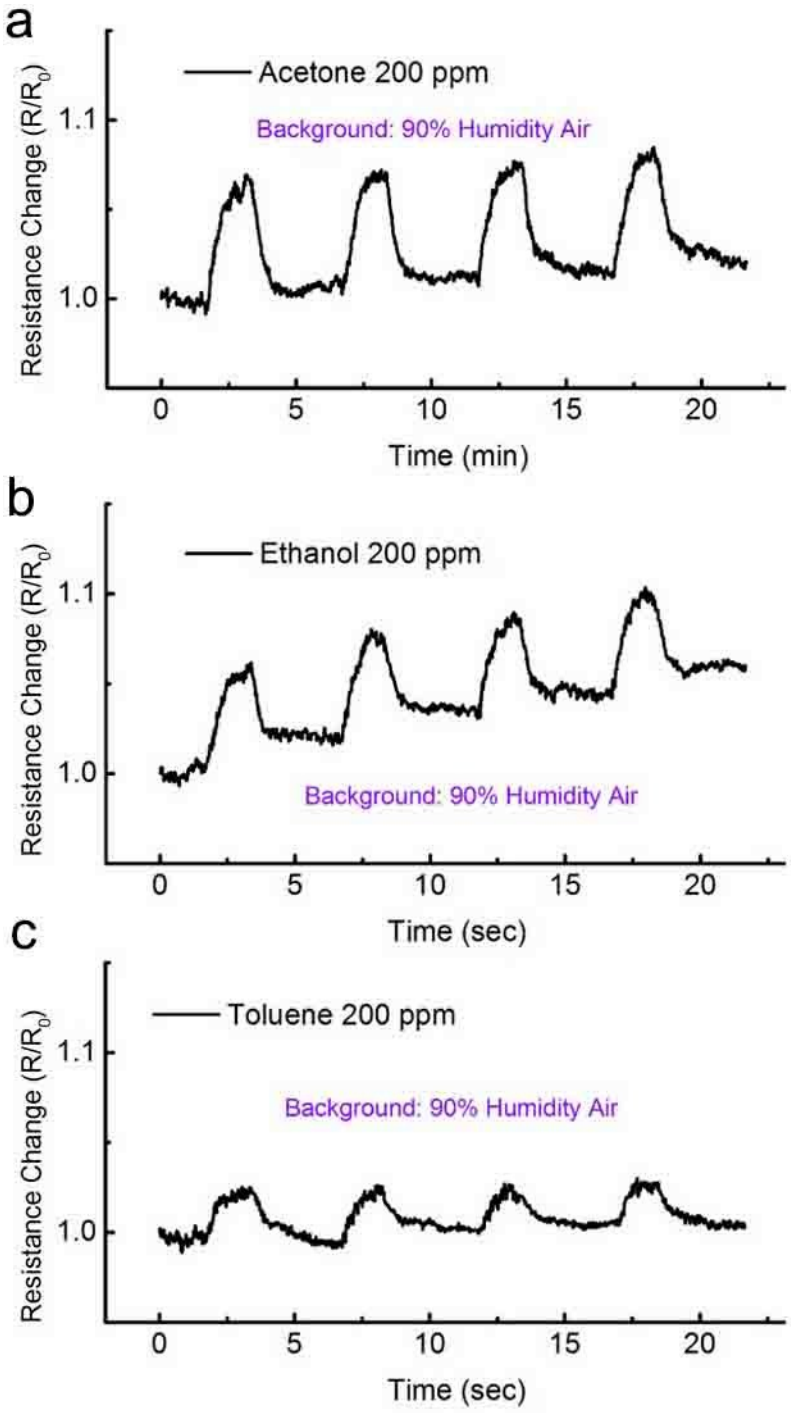

Figure S14. Comparison of responses of $V_4C_3T_x$ sensor in acetone (a), ethanol (b) and eoluene (c) at 200 ppm, under 90% relative humidity air background.

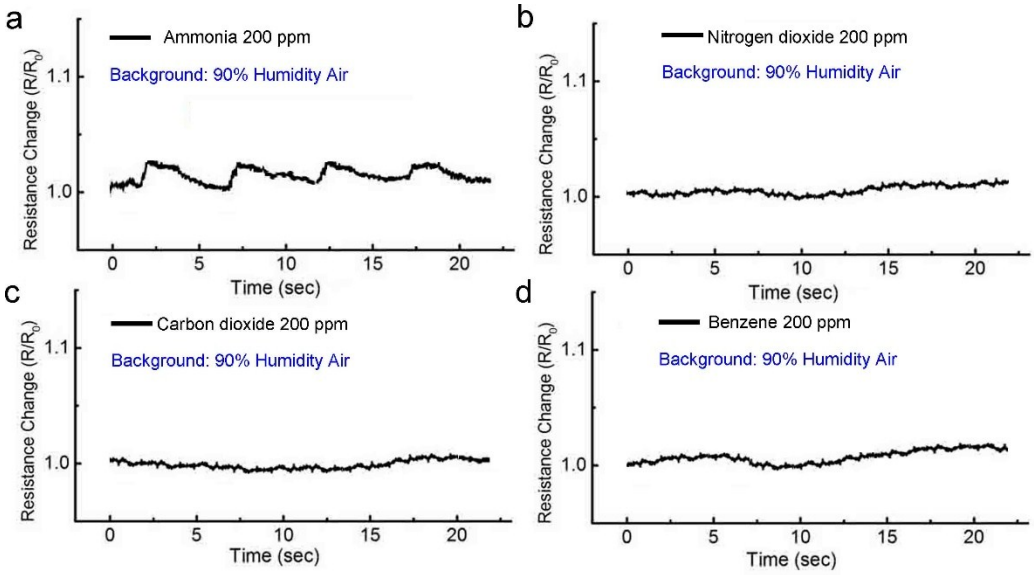

Figure S15. Comparison of responses of $V_4C_3T_x$ sensor in ammonia (a), nitrogen dioxide (b), carbon dioxide (c) and benzene (d) at 200 ppm, under 90% relative humidity air background.

Table S1. EDS result of V_4AlC_3

Point 1					Point 2			
Element	Weight%	Atomic%	Formula		Element	Weight%	Atomic%	Formula
V K	76.94	50.63	4		V K	76.60	50.70	4
Al K	9.68	12.03	0.95		Al K	10.35	12.93	1.02
C K	13.38	37.34	2.95		C K	13.05	36.37	2.87
Totals	100.0				Totals	100.0		
Point 3					Point 4			
Element	Weight%	Atomic%	Formula		Element	Weight%	Atomic%	Formula
V K	77.21	51.02	4		V K	76.25	50.00	4
Al K	9.41	11.73	0.92		Al K	10.40	12.88	1.03
C K	13.38	37.25	2.94		C K	13.35	37.12	2.97
Totals	100.0				Totals	100.0		
Point 5					Point 6			
Element	Weight%	Atomic%	Formula		Element	Weight%	Atomic%	Formula

V K	77.32	51.41	4		V K	76.41	50.06	4
Al K	9.83	12.34	0.96		Al K	10.12	12.52	1.00
C K	12.85	36.25	2.82		C K	13.41	37.42	2.99
Totals	100.0				Totals	100.0		
Average formula: $V_4Al_{0.98(4)}C_{2.92(6)}$								

Table S2. EDS result of $V_4C_3T_x$

Point 1					Point 2			
Element	Weight%	Atomic%	Formula		Element	Weight%	Atomic%	Formula
V K	83.63	54.64	4		V K	85.14	57.47	4
C K	16.37	45.36	3.32		C K	14.86	42.53	2.96
Totals	100.0				Totals	100.0		
Point 3					Point 4			
Element	Weight%	Atomic%	Formula		Element	Weight%	Atomic%	Formula
V K	85.44	58.06	4		V K	83.39	54.20	4
C K	14.56	41.96	2.89		C K	16.61	45.8	3.38
Totals	100.0				Totals	100.0		
Point 5					Point 6			
Element	Weight%	Atomic%	Formula		Element	Weight%	Atomic%	Formula
V K	83.26	53.98	4		V K	85.75	56.65	4
C K	16.74	46.02	3.41		C K	14.25	43.35	2.82
Totals	100.0				Totals	100.0		
Average formula: $V_4C_{3.1(3)}$								